Escape Ratio Contributes More Than Fluorescence Yield to SIF–GPP Relationship Over Crops and Rainforest

Wenhui Yan, Yelu Zeng, *Member, IEEE*, Xinhong Zhang, Weike Zhao, Yongyuan Gao, Yachang He, and Dalei Hao

***Abstract*— Solar-induced chlorophyll fluorescence (SIF) is an effective indicator to track the gross primary productivity (GPP). However, there is still a lack of a clear understanding for the contribution of physiological and structural factors to the SIF–GPP relationship at the canopy scale. To quantify the influence of different SIF components, particularly the photon escape ratio (f_{esc}) and fluorescence yield (Φ_F), on the SIF–GPP relationship, this study evaluated the performance of various vegetation indices (VIs), SIF components, light use efficiency (LUE), and GPP over two typical biomes (crops and rainforest), using a range of satellite remote sensing products. In August of each year from 2018 to 2020, both SIF and GPP over United States (U.S.) Corn Belt are higher than those over the Amazon rainforest, attributed to the consistent pattern of higher f_{esc} and LUE over crops than over rainforest, as well as Φ_F. Furthermore, the structural signals represented by f_{esc} ($R = 0.41$–0.64) can better capture the LUE variations than Φ_F ($R = 0.10$–0.30) for each biome. This study highlights that f_{esc}, determined by canopy structure, has great potential to capture LUE and GPP changes within and across biomes.**

***Index Terms*— Canopy structure, escape ratio, gross primary productivity (GPP), light use efficiency (LUE), solar-induced chlorophyll fluorescence (SIF), vegetation indices (VIs).**

I. Introduction

Accurately estimating gross primary productivity (GPP), which represents the overall quantity of carbohydrates synthesized by plants via photosynthesis, is essential for investigating terrestrial carbon cycles [1]. Advances in remote sensing of solar-induced chlorophyll fluorescence (SIF) have shown great potential of capturing GPP at large scales. SIF is an optical signal emitted within the spectral wavelength range of 650–850 nm from the chlorophyll a molecule present in vegetation [2]. The existing studies have indicated that SIF is closely related to GPP at the leaf, canopy, and ecosystem scales [3], [4].

Mechanically, SIF at the top of the canopy can be separated into three components: absorbed photosynthetically active radiation (APAR), physiological SIF emission yield of the whole canopy (Φ_F), and the escape ratio of photons from the canopy (f_{esc}). Previous studies suggested that the relationship between SIF and GPP is determined jointly by the shared term of APAR and $\mathrm{SIF}_{\mathrm{yield}}$($\mathrm{SIF}_{\mathrm{yield}} = \mathrm{SIF/APAR}$)–light use efficiency (LUE) relationship [5]. At the canopy scale, APAR can explain the linear relationship between GPP and SIF to some extent [6]. However, how the $\mathrm{SIF}_{\mathrm{yield}}$–LUE relationship varies and further influences the SIF–GPP correlation are still unclear. $\mathrm{SIF}_{\mathrm{yield}}$ is jointly determined by Φ_F and f_{esc}. Seasonally, a positive correlation between f_{esc} and LUE contributes to the SIF–GPP relationship, while Φ_F shows a low correlation to LUE at a few crop sites [5]. Nonetheless, under drought conditions, Φ_F can track variations in LUE, assisting SIF in estimating GPP [7]. These researches have demonstrated that both Φ_F and f_{esc} are related to LUE, thereby affecting the estimation of GPP by SIF. However, the existing investigations are mostly at site scales and mainly focus on structurally uniform crops, with a lack of analysis at regional scales and complexly structured ecosystems, such as rainforest. The relative contributions of Φ_F and f_{esc} to the SIF–GPP relationship at large scales remain underinvestigated, particularly given that the SIF–GPP relationship exhibits variations among various biomes [8].

Previous research revealed that the shadows generated by complex forest structure had larger impacts on SIF magnitude, resulting in the SIF of United States (U.S.) Corn Belt being larger than that of the Amazon rainforest in August, despite the latter having a larger leaf area index (LAI) [9]. Similarly, GPP also exhibited higher values in U.S. Corn Belt compared to the Amazon rainforest [10], showing a similar pattern to SIF. Nevertheless, the underlying drivers of the similar spatial patterns of SIF and GPP in these two biomes and the roles of Φ_F and f_{esc} are still unclear.

The objectives of this study are twofold: first, to investigate the roles of Φ_F and f_{esc} in the contrasting pattern across biomes with distinct canopy structures (i.e., U.S. Corn Belt and the Amazon rainforest); and second, to evaluate the contributions of Φ_F and f_{esc} to the $\mathrm{SIF}_{\mathrm{yield}}$–LUE relationship within each biome. Specifically, we analyzed and compared SIF, SIF components, GPP, LUE, and various vegetation indices (VIs) within and across the two biomes using a series of remote sensing products.

Manuscript received 21 May 2024; revised 12 July 2024; accepted 16 July 2024. Date of publication 23 July 2024; date of current version 15 August 2024. This work was supported in part by the National Natural Science Foundation of China under Grant 42271361 and in part by Chinese Universities Scientific Fund. *(Corresponding author: Yelu Zeng.)*

Wenhui Yan, Yelu Zeng, Xinhong Zhang, Weike Zhao, Yongyuan Gao, and Yachang He are with the College of Land Science and Technology, China Agricultural University, Beijing 100083, China (e-mail: zengyelu@163.com).

Dalei Hao is with the Atmospheric, Climate, and Earth Sciences Division, Pacific Northwest National Laboratory, Richland, WA 99354 USA (e-mail: dalei.hao@pnnl.gov).

Digital Object Identifier 10.1109/LGRS.2024.3432820

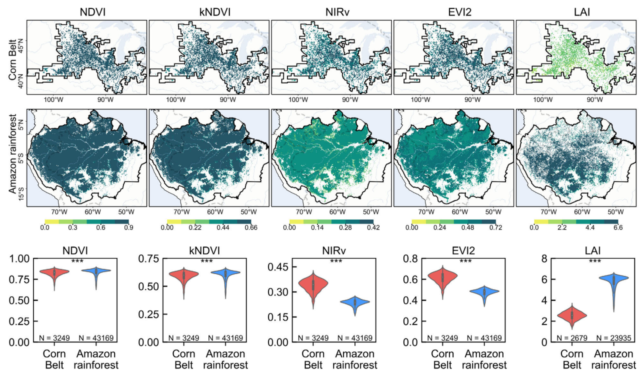

Fig. 1. Comparison of NDVI, kNDVI, NIRv, EVI2, and LAI across U.S. Corn Belt and the Amazon rainforest. The violin plots exhibit the quartiles and mean values of variables, showcasing their distribution patterns. Statistical significance level is denoted as: "***" for $p < 0.001$, "**" for $p < 0.01$, "*" for $p < 0.05$, "ns" for $p \geq 0.05$, and "N" represents the number of samples.

TABLE I
DETAILS OF THE VEGETATION INDICES IN THIS STUDY

Abbreviation	Name	Equation and derivation
NDVI	Normalized difference vegetation index	$\mathrm{NDVI} = \dfrac{\mathrm{NIR} - \mathrm{Red}}{\mathrm{NIR} + \mathrm{Red}}$
kNDVI	Kernel NDVI	$\mathrm{kNDVI}=\tanh\left(\mathrm{NDVI}^2\right)$
NIRv	Near-infrared reflectance of vegetation	$\mathrm{NIRv}=\dfrac{\mathrm{NIR\text{-}Red}}{\mathrm{NIR+Red}}\times \mathrm{NIR}$
EVI2	Two-band enhanced vegetation index	$\mathrm{EVI2}=2.5\times\dfrac{\mathrm{NIR\text{-}Red}}{\mathrm{NIR}+2.4\times\mathrm{Red}+1}$

II. MATERIALS AND METHODS

A. Study Area

The Amazon rainforest spans the latitudes of 19.6°S–8.6°N and longitudes of 79.7°W–44°W (see Fig. 1). This biome is primarily characterized by its evergreen forest cover and stands as one of the most important land carbon sinks [1].

U.S. Corn Belt is situated between latitudes 37.4°N and 47.7°N and longitudes 105.1°W and 82.1°W (see Fig. 1). In this region, corn and soybeans were uniformly cultivated [19].

B. Datasets and Data Processing

The MODIS MCD43A1.061 product provides the isotropic, volumetric, and geometric model parameters at red (620–670 nm) and NIR (841–876 nm) bands to calculate reflectance at a fixed view geometry of VZA = 0° (view zenith angle) and solar geometry of SZA = 45° (solar zenith angle) with the resolution of daily temporally and 500 m spatially [15], [33]. The normalized reflectance was used to ascertain the four VIs listed in Table I [31].

1) FPAR and LAI Products: The MODIS MCD15A2H.061 product leverages multiple spectral bands from Terra and Aqua satellite data to provide estimates of the fraction of photosynthetically active radiation (FPAR) and LAI with a resolution of eight day and 500 m [11]. We used MODIS products with good quality assurance (QA)/quality control (QC) flags.

2) ERA5-Land: The ERA5 dataset is released by the European Center for Medium-Range Weather Forecasts. The photosynthetically active radiation (PAR) was estimated from this product in all sky conditions [12].

3) TROPOMI SIF: The Copernicus Sentinel-5P TROPOMI mission provides SIF observations with enhanced spatiotemporal resolution [13], [14]. To ensure data quality, observations with far-red (740 nm) daily SIF values not within −2–4 mW/m^2/sr/nm and SIF signal uncertainty greater than 0.55 mW/m^2/sr/nm were excluded. Besides, any SIF observations with cloud fraction over 50% were excluded [23].

4) CEDAR GPP: The effect of atmospheric CO_2 on photosynthesis, known as the CO_2 fertilization effects, increases the canopy-level GPP and LUE [32]. The CEDAR GPP product incorporates this effect using both theoretical and data-driven approaches to generate monthly GPP estimations with a spatial resolution of 0.05° [16].

5) X-BASE GPP: The X-BASE product is the global product of the upgraded FLUXCOM-X framework, providing high-resolution GPP data. In this study, the product at a monthly 0.05° resolution was used. The variability of X-BASE GPP has been demonstrated to be highly consistent with TROPOMI SIF variability [17].

6) Land Cover Datasets: This study used the International Geosphere-Biosphere Program classification layer in the MCD12Q1 product to filter uniform pixels of two different biomes [18]. In the Amazon rainforest, only evergreen broad-leaved forest with tree coverage >60% was selected, and in U.S. Corn Belt, only cultivated land accounting for at least 60% of the land was selected. The USDA NASS Cropland data layer (CDL) was further employed to filter and select only the arable land, where corn was planted that year, which has been shown to classify corn in the Midwest with an accuracy of up to 95% [19].

All data were aggregated monthly temporally and 0.1° spatially, confined to August of each year from 2018 to 2020.

Additionally, to ensure data quality, the top and bottom 2% of all data were removed consistently to mitigate the impact of outliers on the results.

C. Methods

1) BRDF Correction: The directional reflectance is highly sensitive to the sun-target-sensor geometry. The RossThick-LiTransit (RTLT) was employed to normalize this effect to nadir view (VZA = 0° and SZA = 45°), preventing the potential misinterpretation of variations induced by geometry as physiological signals. The RTLT kernel-driven semi-empirical BRDF model has been evidenced to show good fitting capabilities, delivering more precise bidirectional reflectance [20], [21]

$$R(\theta_s, \theta_v, \varphi, \lambda) = f_{\mathrm{iso}}(\lambda) + f_{\mathrm{vol}}(\lambda)K_{\mathrm{vol}}(\theta_s, \theta_v, \varphi) + f_{\mathrm{geo}}(\lambda)K_{\mathrm{geo}}(\theta_s, \theta_v, \varphi) \quad (1)$$

where $R(\theta_s, \theta_v, \varphi, \lambda)$ represents the reflectance at a given wavelength λ, considering the SZA θ_s, the VZA θ_v, and the relative azimuth angle (RAA) φ. The reflectance was obtained by linearly combining three scattering components, expressed as the product of the weights and the corresponding kernels.

The isotropic kernels have a constant weight of 1. The weights $f_{vol}(\lambda)$ and $f_{geo}(\lambda)$ represent the empirical kernel parameters at wavelength λ. The kernels $K_{vol}(\theta_s, \theta_v, \varphi)$ and $K_{geo}(\theta_s, \theta_v, \varphi)$ represent the volume scattering kernel RossThick and the geometric-optical surface scattering kernel LiTransit, respectively.

2) Disentangle the Structural and Physiological Signals of the Canopy-Level SIF: The observed canopy-level SIF is primarily determined by three mechanistic factors: APAR, Φ_F, and f_{esc}. SIF is thus defined as

$$\mathrm{SIF} = \mathrm{APAR} \times \Phi_F \times f_{esc}. \tag{2}$$

APAR denotes the total PAR absorbed by vegetation for photosynthesis and growth and can be estimated by combining the FPAR from the MCD15A2H.061 product and PAR from the ERA-5 reanalysis

$$\mathrm{APAR} = \mathrm{PAR} \times \mathrm{FPAR}. \tag{3}$$

f_{esc} is a new physical parameter introduced in radiative transfer theory. In this study, a previously well-validated method based on the spectral invariants theory was adopted, whereby f_{esc} in the far-red band was estimated through [22]

$$f_{esc} \approx \frac{\mathrm{NIRv}}{\mathrm{FPAR}}. \tag{4}$$

Φ_F was calculated using SIF divided by NIRvP, which is the substitute for nonphysiological signals [23]. Crucially, noting that NIRv should be adjusted to the same direction as observed SIF before multiplying by instantaneous PAR for the NIRvP estimation

$$\Phi_F \approx \frac{\mathrm{SIF}}{\mathrm{NIRv} \times \mathrm{PAR}}. \tag{5}$$

3) Estimating LUE: GPP is expressed as a semi-empirical LUE framework comprising APAR and LUE [24]. Then, LUE was calculated as

$$\mathrm{LUE} = \frac{\mathrm{GPP}}{\mathrm{APAR}}. \tag{6}$$

4) Statistical Analysis: Across biomes, the analysis of variance (ANOVA) was primarily employed to compare the mean values of data between biomes for statistically significant differences.

Within each biome, correlation evaluations were conducted utilizing the Pearson correlation coefficient (R), with the assessment of statistical significance executed through a two-sided t-test, employing a 95% confidence interval. Linear regression analysis between variables was also conducted.

III. Results

A. f_{esc} Distorts the Interpretation of VIs

Except for NDVI and kNDVI, which show minor differences between the two biomes, with the values of (mean ± s.d., 0.82 ± 0.04, 0.59 ± 0.04) in U.S. Corn Belt and (0.83 ± 0.04, 0.60 ± 0.05) in the Amazon rainforest, respectively, NIRv (0.34 ± 0.04) and EVI2 (0.61 ± 0.05) exhibit higher values in U.S. Corn Belt compared to the Amazon rainforest characterized by complex canopy structure, where NIRv (0.23 ± 0.02) and EVI2 (0.47 ± 0.03) were lower (see Fig. 1).

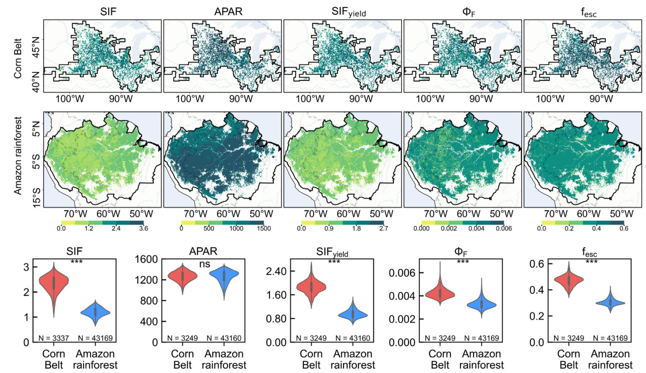

Fig. 2. Comparison of SIF (mW/m^2/nm/sr), APAR (μmol/m^2/s), SIF$_{yield}$ (mW·s/μm/sr/μmol), Φ_F (mW·s/nm/sr/μmol photons), and f_{esc} (unitless) between U.S. Corn Belt and the Amazon rainforest.

Previous studies have demonstrated the hypothesis that complex canopy structure can distort the interpretation of vegetation greenness [9]. Our research findings also demonstrate the important role of f_{esc}, indicating that high VIs and low LAI (2.53 ± 0.38) in uniform crops but with high f_{esc} (0.47 ± 0.04), while low VIs and high LAI (5.75 ± 0.67) in rainforest with low f_{esc} (0.30 ± 0.03) (see Fig. 2).

B. Contrasting Patterns of SIF and SIF Components

The APAR over U.S. Corn Belt (1264.44 μmol/m^2/s) and the Amazon rainforest (1262.50 μmol/m^2/s) exhibits minimal difference. SIF and SIF$_{yield}$, as well as Φ_F and f_{esc}, consistently show that U.S. Corn Belt is higher than the Amazon rainforest, albeit to varying degrees (see Fig. 2).

The SIF of U.S. Corn Belt (2.32 mW/m^2/nm/sr) exceeds that of the Amazon rainforest (1.20 mW/m^2/nm/sr) by 94.5%. Similarly, SIF$_{yield}$ in the former (1.86 mW·s/μm/sr/μmol) also surpasses the latter (0.95 mW·s/μm/sr/μmol) by 94.7%. Although the relative differences in Φ_F (28.5%) and f_{esc} (53.9%) were not as pronounced as those in SIF and SIF$_{yield}$, it still manifests that Φ_F and f_{esc} of the former (0.0042 mW·s/nm/sr/μmol, 0.47) were higher than those of the latter (0.0033 mW·s/nm/sr/μmol, 0.30) (see Fig. 2).

C. GPP and LUE Differences Between Biomes

Between the two biomes, GPP and LUE show significant differences (ANOVA: $p < 0.001$) (see Fig. 3). The X-BASE GPP indicates that U.S. Corn Belt was approximately twice that of the Amazon rainforest, yielding a similar ratio of 2.00 for LUE. Similarly, both CEDAR GPP and CEDAR LUE show that the crops exceeded the rainforest, with GPP and LUE values exhibiting ratios of 1.46 and 1.44, respectively (see Fig. 3).

CEDAR GPP shows higher values in the rainforest than X-BASE GPP, with correspondingly higher LUE, which may

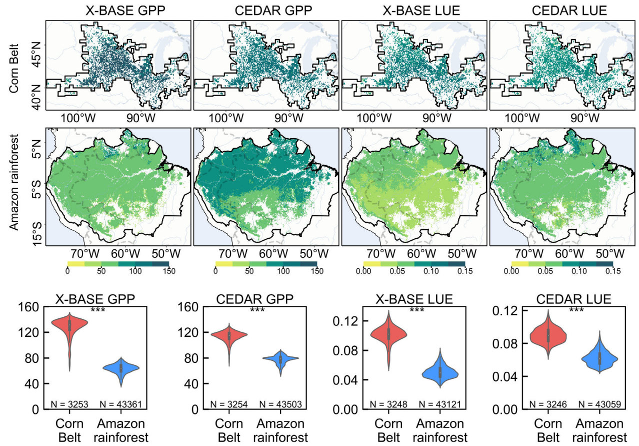

Fig. 3. Comparison of GPP (μmol/m^2/s) and LUE (mol CO_2/mol photons) between U.S. Corn Belt and the Amazon rainforest. The X-BASE LUE and CEDAR LUE were calculated from the corresponding GPP products.

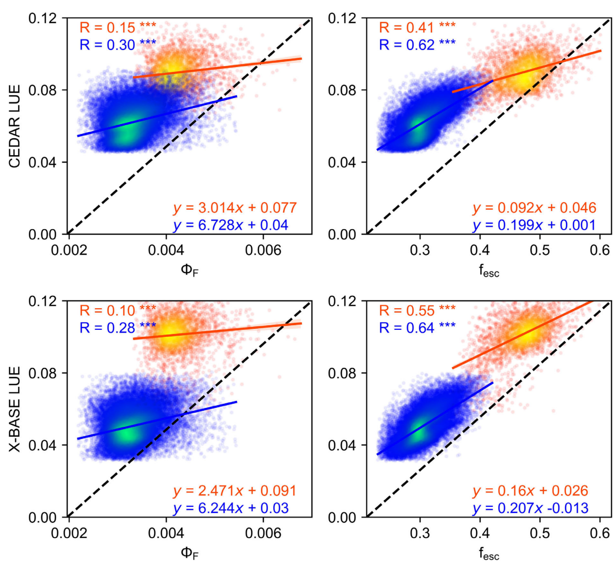

Fig. 4. Comparison of the correlation of Φ_F (mW·s/nm/sr/μmol photons) and f_{esc} (unitless) with CEDAR LUE and X-BASE LUE for 2018–2020, in August, in U.S. Corn Belt (the red one) and the Amazon rainforest (the blue one). The error bars represent 95% confidence intervals. LUE is in the units of mol CO_2/mol photons.

be caused by considering the CO_2 fertilization effect favoring GPP estimation for C3 vegetation [16].

D. Separating the Structural and Physiological Contributions

To directly assess the contributions of each component within each biome, the correlations between Φ_F, f_{esc}, and LUE were further quantified (see Fig. 4). Our analysis revealed that in both biomes, the correlations between f_{esc} and LUE (0.41–0.64) were greater than those between Φ_F and LUE (0.10–0.30). These findings revealed that there was a moderate positive correlation between f_{esc} and LUE, while the correlation between Φ_F and LUE was relatively weak in each biome.

IV. Discussion

A. Analyzing Experimental Results

In comparing the SIF patterns between the two biomes, this study shows that APAR differences are minimal, while SIF_{yield} is higher in U.S. Corn Belt and relatively lower in the Amazon rainforest. The SIF_{yield} pattern was more similar to SIF than to APAR, suggesting a greater contribution of SIF_{yield} to SIF, consistent with previous studies [25]. This performance was due to the combined contributions of f_{esc} and Φ_F, both of which were higher in U.S. Corn Belt than in the Amazon rainforest [26]. The difference in f_{esc} (53.9%) between the two biomes was larger than that of Φ_F (28.5%) and more closely matched the difference in SIF (94.5%), and thus, f_{esc} difference may contribute more to the SIF_{yield} and SIF patterns. For GPP, the similar APAR between biomes indicates that differences in GPP among biomes were mainly controlled by LUE. This analysis suggests that the contrasting SIF–GPP patterns were determined by a complicated relationship between Φ_F, f_{esc}, and LUE [29].

In each biome, there was a highly positive correlation between f_{esc} and LUE in both the structurally uniform crops and the complex rainforest. This correlation surpassed that between Φ_F and LUE, consistent with earlier studies focused on the site scales and crops [5], while now corroborated across regional scales and complexly structured ecosystems. Moreover, building upon past findings that a positive f_{esc}–LUE relationship can strengthen the SIF–GPP relationship [30], this regional investigation reveals the importance of f_{esc} in explaining SIF–GPP variations across different ecosystems, further underscoring the relationship between f_{esc} and LUE, which may benefit the large-scale GPP estimations.

From the perspective of vegetation physiology, photosynthetic activity and even leaf shape at the leaf level will change under different conditions (e.g., light saturation, stress) [27], [28]. Together, the responses of the individual leaves across the canopy form the coupling mode of f_{esc}, Φ_F, and LUE. Besides, product uncertainties remain, especially under different environmental conditions, and these uncertainties and their further effects should be taken into account. For example, FPAR directly influences APAR, which further affect the quantification of the relationship between GPP and SIF [34]. During the study period, the regions were not subjected to any large-scale environmental stresses, and thus, further investigation is needed to explore the corresponding SIF–GPP patterns during stress conditions.

B. Limitations and Prospects

Temporally, due to the short operational span of TROPOMI, the analysis was restricted from 2018 to 2020. Moreover, this study focused on August, a period of peak ecosystem activity for U.S. Corn Belt (July and August) in the northern hemisphere, to enable the comparisons of different regions globally at the same time. Further extension of longer time series will allow us to explore interannual and long-term changes in vegetation canopy structure and physiological components, contributing to a more comprehensive understanding.

Spatially, this study mainly focuses on two typical biomes: evergreen broadleaf forest and corn belt. In future, we plan to incorporate additional biomes under varying climate zones to study potential differences in the ability of f_{esc} capturing LUE, which will help us better understand the SIF–GPP relationship and benefit the large-scale GPP mapping.

V. Conclusion

Starting from the perspective that f_{esc} distorts the interpretation of VIs, we conducted a comparative analysis of SIF, SIF components, GPP, and LUE in two typical biomes characterizing different canopy complexities. This study reveals that SIF and GPP in summer crops were higher than those in tropical rainforest, with both f_{esc} and Φ_F contributing positively to this pattern. Furthermore, both Φ_F and f_{esc} within each biome show positive correlations with LUE, while the correlation between f_{esc} (0.41–0.64) and LUE surpassed that of Φ_F (0.10–0.30) and LUE, indicating that f_{esc} better captured the variations in LUE. This letter emphasizes the important contribution of f_{esc} to the SIF–GPP relationship. We advocate for increased attention to f_{esc}, representing canopy structure importantly.

References

[1] C. Beer et al., "Terrestrial gross carbon dioxide uptake: Global distribution and covariation with climate," *Science*, vol. 329, no. 5993, pp. 834–838, Aug. 2010.

[2] H. K. Lichtenthaler, C. Buschmann, U. Rinderle, and G. Schmuck, "Application of chlorophyll fluorescence in ecophysiology," *Radiat. Environ. Biophys.*, vol. 25, no. 4, pp. 297–308, Dec. 1986.

[3] J. D. Wood, T. J. Griffis, J. M. Baker, C. Frankenberg, M. Verma, and K. Yuen, "Multiscale analyses of solar-induced florescence and gross primary production," *Geophys. Res. Lett.*, vol. 44, no. 1, pp. 533–541, Jan. 2017.

[4] Y. Sun et al., "Overview of solar-induced chlorophyll fluorescence (SIF) from the orbiting carbon observatory-2: Retrieval, cross-mission comparison, and global monitoring for GPP," *Remote Sens. Environ.*, vol. 209, pp. 808–823, May 2018.

[5] B. Dechant et al., "Canopy structure explains the relationship between photosynthesis and sun-induced chlorophyll fluorescence in crops," *Remote Sens. Environ.*, vol. 241, May 2020, Art. no. 111733.

[6] Z. Li et al., "Solar-induced chlorophyll fluorescence and its link to canopy photosynthesis in maize from continuous ground measurements," *Remote Sens. Environ.*, vol. 236, Jan. 2020, Art. no. 111420.

[7] J. Chen, X. Liu, S. Du, Y. Ma, and L. Liu, "Effects of drought on the relationship between photosynthesis and chlorophyll fluorescence for maize," *IEEE J. Sel. Topics Appl. Earth Observ. Remote Sensor*, vol. 14, pp. 11148–11161, 2021.

[8] H. Gao et al., "Global analysis of the relationship between reconstructed solar-induced chlorophyll fluorescence (SIF) and gross primary production (GPP)," *Remote Sens.*, vol. 13, no. 14, p. 2824, Jul. 2021.

[9] Y. Zeng et al., "Structural complexity biases vegetation greenness measures," *Nature Ecol. Evol.*, vol. 7, no. 11, pp. 1790–1798, Sep. 2023.

[10] R. Chen, L. Liu, X. Liu, and U. Rascher, "CMLR: A mechanistic global GPP dataset derived from TROPOMIS SIF observations," *J. Remote Sens.*, vol. 4, p. 0127, Jan. 2024.

[11] R. Myneni and T. Park, 2021, "MODIS/Terra+ Aqua leaf area index/FPAR 4-day L4 global 500 m SIN grid V061," Land Processes Distributed Active Archive Center (LP DAAC), Sioux Falls, SD, USA, 2021.

[12] K. J. McCree, "Test of current definitions of photosynthetically active radiation against leaf photosynthesis data," *Agricult. Meteorol.*, vol. 10, pp. 443–453, Jan. 1972.

[13] L. Guanter et al., "The TROPOSIF global sun-induced fluorescence dataset from the Sentinel-5P TROPOMI mission," *Earth Syst. Sci. Data*, vol. 13, no. 11, pp. 5423–5440, Nov. 2021.

[14] P. Köhler, C. Frankenberg, T. S. Magney, L. Guanter, J. Joiner, and J. Landgraf, "Global retrievals of solar-induced chlorophyll fluorescence with TROPOMI: First results and intersensor comparison to OCO-2," *Geophys. Res. Lett.*, vol. 45, no. 19, pp. 10456–10463, Oct. 2018.

[15] C. Schaaf and Z. Wang. (2021). *MODIS/Terra+Aqua BRDF/Albedo Model Parameters Daily L3 Global-500m V061. 2021, Distributed by NASA EOSDIS Land Processes Distributed Active Archive Center*. Accessed: May 5, 2024. [Online]. Available: https://doi.org/10.5067/MODIS/MCD43A1.061

[16] Y. Kang et al., "CEDAR-GPP: Spatiotemporally upscaled estimates of gross primary productivity incorporating CO_2 fertilization," *Earth Syst. Sci. Data Discuss.*, pp. 1–51, Oct. 2023.

[17] J. A. Nelson et al., *X-Base: The First Terrestrial Carbon and Water Flux Products From an Extended Data-Driven Scaling Framework, FLUXCOM-X*. Munich, Germany: EGUsphere, 2024.

[18] M. A. Friedl et al., "Global land cover mapping from MODIS: Algorithms and early results," *Remote Sens. Environ.*, vol. 83, nos. 1–2, pp. 287–302, 2002.

[19] C. Boryan, Z. Yang, R. Mueller, and M. Craig, "Monitoring U.S. agriculture: The U.S. department of agriculture, national agricultural statistics service, cropland data layer program," *Geocarto Int.*, vol. 26, no. 5, pp. 341–358, Aug. 2011, doi: 10.1080/10106049.2011.562309.

[20] X. Li et al., "Derivation and validation of a new kernel for kernel-driven BRDF models," *Proc. SPIE*, vol. 3868, pp. 368–379, Dec. 1999.

[21] F. Gao, X. Li, A. Strahler, and C. Schaaf, "Evaluation of the li transit kernel for BRDF modeling," *Remote Sens. Rev.*, vol. 19, nos. 1–4, pp. 205–224, Dec. 2000.

[22] Y. Zeng, G. Badgley, B. Dechant, Y. Ryu, M. Chen, and J. A. Berry, "A practical approach for estimating the escape ratio of near-infrared solar-induced chlorophyll fluorescence," *Remote Sens. Environ.*, vol. 232, Oct. 2019, Art. no. 111209.

[23] B. Dechant et al., "NIRVP: A robust structural proxy for sun-induced chlorophyll fluorescence and photosynthesis across scales," *Remote Sens. Environ.*, vol. 268, Jan. 2022, Art. no. 112763.

[24] J. L. Monteith, "Solar radiation and productivity in tropical ecosystems," *J. Appl. Ecol.*, vol. 9, no. 3, pp. 747–766, Dec. 1972.

[25] C. Wang et al., "Satellite footprint data from OCO-2 and TROPOMI reveal significant spatio-temporal and inter-vegetation type variabilities of solar-induced fluorescence yield in the U.S. midwest," *Remote Sens. Environ.*, vol. 241, May 2020, Art. no. 111728.

[26] G. Miao et al., "Sun-induced chlorophyll fluorescence, photosynthesis, and light use efficiency of a soybean field from seasonally continuous measurements," *J. Geophys. Res., Biogeosci.*, vol. 123, no. 2, pp. 610–623, Feb. 2018.

[27] C. D. Holder, "The relationship between leaf hydrophobicity, water droplet retention, and leaf angle of common species in a semi-arid region of the western United States," *Agricult. Forest Meteorol.*, vol. 152, pp. 11–16, Jan. 2012.

[28] G. S. Schlau-Cohen and J. Berry, "Photosynthetic fluorescence, from molecule to planet," *Phys. Today*, vol. 68, no. 9, pp. 66–67, Sep. 2015.

[29] R. Chen, L. Liu, X. Liu, Z. Liu, L. Gu, and U. Rascher, "Improving estimates of sub-daily gross primary production from solar-induced chlorophyll fluorescence by accounting for light distribution within canopy," *Remote Sens. Environ.*, vol. 300, Jan. 2024, Art. no. 113919.

[30] L. Liu et al., "Estimating maize GPP using near-infrared radiance of vegetation," *Sci. Remote Sens.*, vol. 2, Dec. 2020, Art. no. 100009.

[31] Y. Zeng et al., "Optical vegetation indices for monitoring terrestrial ecosystems globally," *Nature Rev. Earth Environ.*, vol. 3, no. 7, pp. 477–493, May 2022.

[32] C. Chen, W. J. Riley, I. C. Prentice, and T. F. Keenan, "CO_2 fertilization of terrestrial photosynthesis inferred from site to global scales," *Proc. Nat. Acad. Sci. USA*, vol. 119, no. 10, Mar. 2022, Art. no. e2115627119.

[33] R. Dalagnol et al., "AnisoVeg: Anisotropy and nadir-normalized MODIS multi-angle implementation atmospheric correction (MAIAC) datasets for satellite vegetation studies in South America," *Earth Syst. Sci. Data*, vol. 15, no. 1, pp. 345–358, Jan. 2023.

[34] K. Yan, X. Zhang, R. Peng, S. Gao, and J. Liu, "The impact of quality control methods on vegetation monitoring using MODIS FPAR time series," *Forests*, vol. 15, no. 3, p. 553, Mar. 2024.